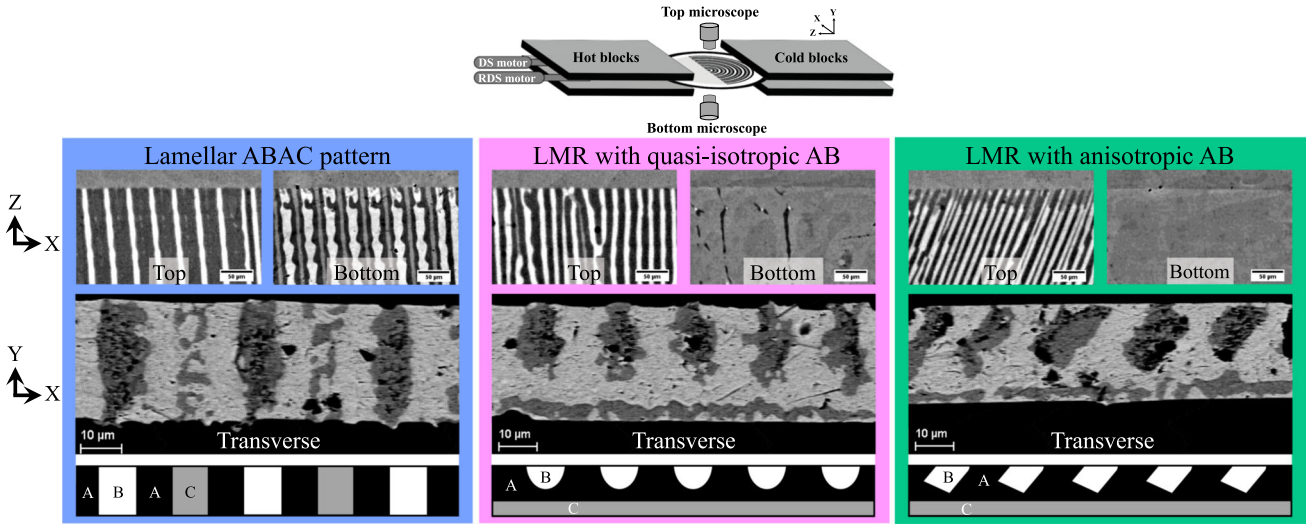
ORIGINAL RESEARCH ARTICLE

On the Effect of Interphase Boundary Energy Anisotropy on Morphologies: A New Type of Eutectic Grain Observed in a Three-Phase Eutectic System

SAMIRA MOHAGHEGHI and MELIS ŞEREFOĞLU

Eutectic microstructures are dramatically affected by the anisotropy in interphase boundary energy. Depending on this anisotropy function, different eutectic grains may grow simultaneously at the same experimental conditions. In all reported quasi-isotropic and anisotropic two-phase and three-phase eutectic grains in thin samples, lamellar morphology is observed and the microstructure is essentially two dimensional (2D), since the interphase boundaries are perpendicular to the sample walls. Using the β(In)–In_2Bi–γ(Sn) system and real-time solidification experiments in thin samples, we introduce a unique and new type of anisotropic three-phase eutectic grain, entitled here as ''Laminated Matrix with Rods (LMR).'' In this grain, due to the anisotropy in In_2Bi/γ(Sn) interphase boundary, the evolving phases, and hence, the microstructures observed through the two glass plates of the thin sample are completely different, despite the strong confinement effect. During rotating directional solidification (RDS) experiments, the morphology or the aspect ratio of all phases changes periodically and drastically. Specifically, In_2Bi, β(In), and γ(Sn) phases evolve from all being lamellar perpendicular to the sample walls to the matrix, elongated/trapezoidal rods, and a lamella parallel to the sample walls, respectively. Our experimental results show that these morphological transitions are due to change in the interphase boundary orientation with respect to the growth direction.



https://doi.org/10.1007/s11661-024-07389-6
© The Author(s) 2024

I. INTRODUCTION

WHEN the eutectic phases have nonfaceted solid/liquid interfaces, they can grow easily along all crystallographic directions during solidification. This type of eutectic microstructures is called ''regular'' due to

SAMIRA MOHAGHEGHI is with the Department of Mechanical Engineering, Istinye University, 34396 Sarıyer, Istanbul, Turkey. Melis Şerefoğlu is with the Department of Metallurgical and Materials Engineering, Marmara University, 34854 Maltepe, Istanbul, Turkey. Contact e-mail: mserefoglu@marmara.edu.tr
Manuscript submitted July 7, 2023; accepted March 15, 2024.

Published online: 03 May 2024

having a rather uniform microstructure compared to the ones obtained in irregular eutectic microstructures where at least one phase has faceted solid/liquid interface.[1] Although they are called "regular", depending on the surface energy of the interphase boundary, variety of microstructures are formed and the growth dynamics may exhibit anisotropic behavior as observed in both organic and metallic systems.[2–12] The interphase boundary energy anisotropy, which is a function of orientation of neighboring phases with respect to each other, originates from the fact that the eutectic phases may have dissimilar crystal structures and definitely different lattice parameters. The strength of the interphase anisotropy is a function of these differences in addition to the specific orientation of the neighboring phases with respect to each other. The interface energy functions are traditionally plotted as γ-plot (Wulff plot). Between two phases, with a given orientation relationship (OR), there is only one interface energy function (γ-plot), which is three-dimensional (3D). As a result, only one 3D equilibrium shape can be defined between two phases with a given orientation relationship. If the γ-plot is isotropic, the equilibrium shape will simply be a sphere; however, due to the nature of crystals, both γ-plot and equilibrium shapes can be very complicated.[13] Depending on having minima on the γ-plot or not, the interphases are called anisotropic or isotropic, respectively. If there are minima, depending on their type, different equilibrium shapes can be obtained using the Wulff construction method. In the last decade, two-phase and three-phase eutectic grains in thin sample geometry are classified as quasi-isotropic, nearly-locked, and locked in the case of negligible, non-singular, and singular minima, respectively, in the corresponding γ-plot of the interphase boundary.[3–5,9,11] Quasi-isotropic eutectic grains have negligible anisotropy which does not affect the growth dynamics and hence in these grains, uniform lamellar structure growing in the direction of the imposed temperature gradient (G) is formed. Whereas, in locked grains, the interphase boundary energy is strongly anisotropic and the boundary is aligned toward a direction that corresponds to a minimum energy orientation in γ-plot.[2] Simulations, employing phase-field and dynamic boundary integral methods, confirm the strong locking of the lamellar structure in the presence of anisotropy at the interphase boundary.[14,15] There are still many different anisotropic microstructures observed in regular eutectics that cannot be classified under these categories.

In all these aforementioned grain types reported experimentally and numerically in two-phase CBr_4–C_2Cl_6,[2–4,16] In–In_2Bi,[3,7,16] Al-Al_2Cu[11,17] eutectic systems, three-phase β(In)–In_2Bi–γ(Sn)[5,9,18–20] eutectic system, and simulations,[15,21,22] irrespective of the anisotropy type and strength, the growth morphology of all the phases was always lamellar in thin samples. This means that all the interphase boundaries are nearly normal to the sample walls (glass plates), which results in forming essentially two-dimensional (2D) lamellar microstructure. For regular eutectic structures, it is shown that the morphology of the phases, *i.e.*, rod or lamella, depends on the phase fraction,[23] sample confinement,[24–27] velocity,[27] and thermal field.[28] Simultaneous growth of rod and lamellar morphologies is also reported.[27–30] Recently, Khanna *et al.* bring evidence that lamellar morphology is observed in the presence of interphase boundary anisotropy, although rod morphology would be expected due to the low fraction of the minority phase.[30] Despite numerous recent studies about the effect of the interphase boundary anisotropy on the solidification microstructures, its influence on the growth morphology of the phases is not clear.

In this work, using three-phase β(In)–In_2Bi–γ(Sn) alloy system and real-time directional solidification (DS) and rotating directional solidification (RDS) experiments, we introduce a unique and new class of anisotropic eutectic grain, entitled here as "Laminated Matrix with Rods" (LMR), which has remarkable features, growth dynamics, and morphological transitions. Observation of morphological transitions, while keeping all the alloy and experimental parameters constant, brings clear evidence of the effect of the interphase boundary energy anisotropy on the growth morphology. By performing systematic investigation on the microstructure evolution of LMR eutectic grains in real time, the origin and the mechanisms of the morphological transitions are proposed. Interestingly, LMR grains are observed in majority of the RDS experiments performed with this system.

II. EXPERIMENTAL METHODS

The three-phase eutectic alloy at ternary eutectic composition (In–20.7 at.pct Bi–19.1 at.pct Sn[31]) was prepared from elemental In, Bi, and Sn having a purity level of 99.999 pct by melting and mixing under argon atmosphere. Three solid phases forming at this ternary eutectic point are β(In), In_2Bi, and γ(Sn). The sample containers consist of two approximately 300 μm-thick glass plates separated by 13 or 23 μm-thick Mylar spacers. To prepare the sample, the glass sample container was filled by the molten alloy with argon pressure, and cooled rapidly to obtain a fine as-cast microstructure. The orientations of phases are determined by nucleation occurring during this cooling process. The actual sample thickness is generally higher than Mylar thickness since there may be an extra space between the glass plates and Mylar. The reported sample thicknesses in this article are the Mylar thickness (δ) values.

Horizontal Bridgman-type setups, namely DS and RDS, are used to investigate the solidification microstructures in situ. The RDS setup is demonstrated schematically in Figure 1 and a real image of the setup showing its components is given in the supplementary material 1. In the frame of the experimental setup, the X, Y, and Z axes of the Cartesian coordinate represent the sample width, sample thickness, and the direction of the imposed temperature gradient, respectively. In the RDS setup, a unidirectional temperature gradient is established between hot and cold blocks. While the

temperature of hot blocks is measured by PT-100s and controlled by PID controllers, the temperature of the cold blocks is controlled by a circulator. The temperatures of the hot and cold blocks are arranged such that the solidification front is kept at the gap between the hot and cold blocks to be able to observe the solidification dynamics in real time. Temperature fluctuations, which may severely affect the solidification front dynamics, are avoided with the use of insulators on top and bottom of the copper blocks and by minimizing air flow around the setup. The sample is fixed to a sample holder and sandwiched between top and bottom copper blocks to maximize the thermal stability. We recall that within the RDS setup, there are two different motors and while one motor is used to translate sample directionally in Z-axis, the other one is giving the rotational motion in the XZ plane. The Cartesian coordinate as well as all the components of the system (microscopes, positions of hot and cold blocks, hence, the temperature gradient) are fixed and only the sample moves directionally from hot to cold blocks during DS or rotates within the XZ plane during RDS experiments. More specifically, during RDS, the sample has fixed X, Y, Z positions in the coordinate system and as the sample rotates continuously, the phases are forced to grow in a different direction compared to the one couple seconds ago due to the imposed and fixed temperature gradient. If the grain is quasi-isotropic, crystals can easily grow in any direction. Therefore, the phases and the interphase boundaries follow the rotation and hence, the interphase boundaries left in the solid are circular. However, if the grain is anisotropic, the phases will follow the direction of minima on the γ-plot, not the temperature gradient axis, hence the trace of the interphase boundaries left in the solid will not be circular. Akamatsu *et al.* showed that the trace of the interphase boundaries left in the solid is homothetic to a 2D section of an equilibrium shape.[3,4] Since the observed pattern in β(In)–In_2-Bi–γ(Sn) system is ABAC, there are two interphase boundaries, *i.e.,* A/B and A/C, as shown in Figure 2. As a result, two different γ-plots play decisive roles in microstructure evolution.

Different 3D γ-plots are obtained as a function of OR between the crystalline phases. For a given OR, as a function of crystal orientations and hence, interphase boundary orientation with respect to the XZ plane of the experimental setup, different microstructure evolution dynamics are obtained. During an RDS experiment, the sample is rotated only in XZ plane. Hence, only a 2D cut of a 3D γ-plot, accordingly, a 2D equilibrium shape could be investigated for a given grain. For example, if the γ-plot is isotropic, in other words, the constructed equilibrium shape is a sphere, the equilibrium shape (interphase boundary left in the solid) that will be obtained by rotating the sample in any plane will be a circle. It should be noted here that, during the DS of an anisotropic grain, if the interphase boundary orientation is within the angular range of a circular (unlocked) region on γ-plot, the microstructural features will be similar to the ones observed in an isotropic grain. In other words, the effect of anisotropy on microstructure evolution will not be clearly observable unless the interphase boundary orientation is changed within a constant and directional temperature gradient. Employing RDS technique, this problem is overcome by continuous rotation of the sample in XZ plane within a fixed temperature gradient. Hence, the growth dynamics of different eutectic grain types can be quantitatively characterized in situ as a function of interphase anisotropy.[3,5,9]

In both DS and RDS experiments, after directional melting, the sample is first kept at rest ($V = 0$) in the imposed temperature gradient. At the beginning of RDS experiments, the samples are only directionally solidified in a narrow channel (grain selector) to eliminate the majority of the as-cast grains and to obtain a large grain for quantitative analysis. Unfortunately, neither the orientation of any phase nor the orientation relationships between the phases can be controlled. Orientation of phases (and hence ORs) is determined during the nucleation process occurring right after sample filling. No nucleation is observed after the establishment of three-phase growth front. Therefore, for a given grain, both the phase orientations and orientation relationships stay the same in the channel and during DS and RDS experiments. If the grain obtained is out of interest, it is melted by moving the sample further into the hot blocks and growth started from a different grain after the sample is first kept at rest (as explained at the beginning of this paragraph). Successively, the sample is further directionally solidified until the solidification front reaches the center of rotation.[3] At this time, the directional motion is stopped, and instantaneously, the sample is started to rotate. During the rotation of the sample in counterclockwise (CCW) direction, solidification occurs in clockwise (CW) direction, and vice versa. The circular arrows at the coordinate system on the RDS images show the growth direction. While the sample is rotating, the directional solidification takes place in half of the sample width and the other half undergoes directional melting. Therefore, the solidification microstructure is destroyed in each 180 deg rotation of the sample. However, one can reconstruct a full turn (360 deg) microstructure of the entire sample, called here the RDS pattern, by taking frequent images of the microstructure and merge them in the form of mosaic images to be able to obtain the interphase boundaries left in the solid, *i.e.,* the equilibrium shape. 360 deg rotation of the sample within an imposed temperature gradient corresponds to the rotation of the interphase boundaries over the entire crystallographic orientation in 2D. Since the trace of an interphase boundary extracted from an RDS pattern of a sample that is rotated 360 deg is homothetic to 2D Wulff shape (*i.e.,* the equilibrium shape) of the interphase boundary,[3,4] one can calculate the energy function of the interphase boundary knowing the Wulff shape since the shape is the inner envelope of the γ-plot (Wulff plot) as performed by the authors in Reference 9. During an RDS experiment, a 2D cut of a 3D equilibrium shape is obtained.

The directional solidification velocities (V) and the angular speeds (ω) employed in this study are in the range of $0.08 - 1.00$ μm/s and $0.006 - 0.058$ deg/s, respectively. During RDS, the rotation of the sample

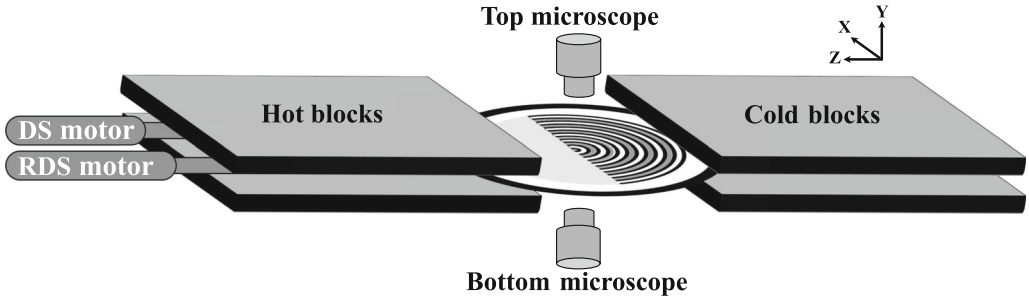


Fig. 1—Schematic representation of the RDS experimental setup and the microscopy system. (DS setup has the same principles with rectangular sample and without RDS motor). During in situ solidification experiments, the *XZ* plane of the microstructure is continuously monitored by two lenses of the microscopes from top and bottom.

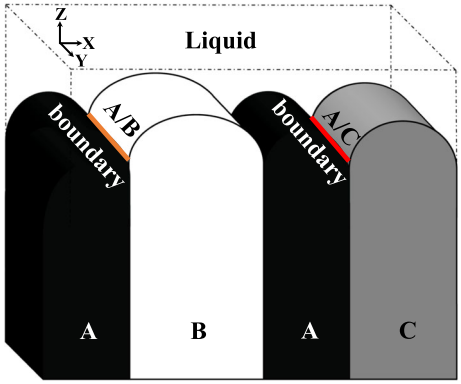


Fig. 2—Schematic representation of the ABAC-type growth pattern. Examples of A/B and A/C interphase boundaries are shown with orange and red lines, respectively. The microstructure within the *XY* plane is observed after post-mortem metallographic preparation (Color figure online).

at a fixed angular speed imposes a velocity-ramp on the solidification front, increasing continuously from center to the edge of the sample. Within this velocity range, even the maximum growth velocity is sufficiently low such that the local equilibrium conditions are maintained at the solidification front. The velocity variation along the solidification front, however, has the typical influence on the microstructure scale but it does not affect the dynamics of microstructure evolution determined by the interphase energy anisotropy.[9] The temperature gradient (G) at the solidification front is measured to be 3.3 and 5.1 K/mm in DS and RDS setups, respectively.

The solidification front during both DS and RDS experiments is observed in real time from both sides of the sample by using a particular microscopy system which is called a double-sided microscope (Figure 1). This system contains one inverted and one upright microscopes which are mounted such that the lenses of both microscopes are observing the same region in the *XZ* plane from top and bottom. In this paper, the images labeled as "top" and "bottom" refer to the microstructures observed from upright and inverted microscopes, respectively. Thanks to this unique microscopy system, since the microstructure is observed from both sides, 2D and 3D features of the microstructure can be detected. In this study, a lamellar structure with boundaries extending from one sample wall to another is called 2D, and in this case, the structure on top and bottom is almost the same. On the other hand, any difference in top and bottom microstructures is hence called 3D. A motorized stage with micrometer resolution is used within this microscopy system to be able to capture images of the whole microstructure from both sides of the sample. It should be mentioned here that there are some black spots in the optical images. These spots are dirt on top of the glass plates; hence, they are neither contaminating the alloy nor affecting the growth dynamics.

Due to the absence of any solid-state transformation at this composition,[20,31,32] the solidification microstructure can be investigated at room temperature by post-mortem analysis. The only difference is the phase fraction of the phases from T_E to T_{room}. The cross-sectional microstructure of a sample, *i.e.,* the *XY* plane, is observed with a back-scattered electron (BSE) detector of SEM. While under the optical microscope, after contrast and brightness enhancement, In_2Bi, β(In), and γ(Sn) appear black, white, and gray, respectively (Figure 2), in BSE images, they are light gray, dark gray, and dark gray. In other words, the color difference between the β(In) and γ(Sn) phases is not distinguishable. Nevertheless, the identity of these phases is confirmed using an energy-dispersive X-ray (EDX) detector of SEM.

III. RESULTS

The basic state in β(In)–In_2Bi–γ(Sn) eutectic system is established to be ABAC pattern (Figure 2) in thin samples[18,19] where A, B, and C refer to In_2Bi, β(In), γ(Sn), respectively. The stability diagram for ABAC pattern and Jackson-Hunt constants of β(In)–In_2Bi–γ(Sn) eutectic system were experimentally obtained.[18] There are only two interphase boundaries in ABAC pattern which are the boundaries between In_2Bi/β(In) phases (A/B) and In_2Bi/γ(Sn) phases (A/C), shown schematically in Figure 2. More specifically, B and C phases are never in contact with each other, except during some transitions[18] such as large-amplitude velocity jumps where ABC pattern forms. Theoretical and numerical study of three-phase lamellar

eutectic patterns in thin samples[22] compared the eutectic growth solutions in ABAC and ABC patterns using a symmetric phase diagram. Using a Jackson–Hunt-type calculation, they derived expressions for the front undercooling as a function of velocity and spacing. It can be seen from the undercooling vs. spacing curves (Figure 16 of Reference. 22) that the diffusion branch of the curve (the right side of the minimum undercooling spacing) has lower undercooling for ABAC pattern than ABC pattern for both of the velocities. More specifically, the formation of ABAC, instead of ABC, reduces the solutal undercooling. The formation of ABAC instead of ABC pattern in β(In)–In_2Bi–γ(Sn) eutectic system could be also attributed to the reduction of the solutal undercooling since both B and C phases contain considerable higher amount of Sn and lower amount of Bi compared to In_2Bi phase.[33] In other words, growing neighboring phases with dissimilar compositions will ease the solute exchange and minimize the diffusion path.

Three distinctive types of three-phase eutectic grains, namely quasi-isotropic, nearly-locked, and locked, were identified and characterized in the β(In)–In_2Bi–γ(Sn) eutectic system by the authors using the RDS technique.[5,9] The microstructural evolution of these grain types during RDS is illustrated in Figure 3. In all these images, while solidification occurs in the left half of the image, melting takes place in the right half of the image. In a quasi-isotropic grain (Figure 3(a)), none of the interphase boundary energies are anisotropic enough to affect the microstructure; thus, floating ABAC pattern evolves throughout the 180 deg rotation of the sample. Floating pattern or floating dynamics refers to a growth type where the triple-point junctions (the junctions where two solids meet the liquid) follow the direction of the imposed temperature gradient during an RDS experiment.[3,4] Floating dynamics are only observed when the interphase boundary energy does not change as a function of rotation. Hence, floating ABAC pattern is observed in quasi-isotropic eutectic grains in addition to the unlocked states of anisotropic grains. On the other hand, the microstructure evolution of the anisotropic grains (Figures 3(b) and (c)) contains several (nearly-) locked states. Following the explanation in References 3, 4, a state is defined as the microstructure obtained within a single eutectic grain in an angular range in the RDS pattern. This angular range corresponds to a specific range in 2D γ-plot and hence, in the equilibrium shape. Depending on the 2D cut of the 3D γ-plot of a eutectic grain obtained during an RDS experiment, the angular range over which the state is persistent is defined (examples are given in Figures 4 and 5 of Reference 4). Within a state, the growth dynamics of the grain is the same. Therefore, the phase growth morphology and solidification microstructure within the angular limits of a state are equivalent and well-distinguishable from the previous and upcoming states of the same grain during RDS. For example, in quasi-isotropic grain, there is only one state. In the nearly-locked grain shown in Figure 3(b), however, there are two nearly-locked states, one unlocked state and transition states between those.

In the identified nearly-locked (Figure 3(b)) and the locked (Figure 3(c)) eutectic grains, the anisotropic interphase boundaries responsible for the (nearly-) locking phenomenon are established to be In_2Bi/γ(Sn) and In_2Bi/β(In), respectively.[5,9] Therefore, the interphase energies of both boundaries can be anisotropic and, depending on the anisotropy function, they give rise to completely different microstructures and solidification dynamics. In these anisotropic grains, within the (nearly-) locked states, the triple-point junctions do not follow the direction of the imposed temperature gradient but instead follow the minimum in the γ-plot. As a result, the traces of interphase boundaries left in the solid are inclined with respect to the temperature gradient and they are straight lines in the RDS pattern unlike circular interphase boundaries observed in quasi-isotropic grains and unlocked states.

A new eutectic grain type is discovered and characterized in this system during DS experiments in thin samples. In this eutectic grain, in strong contrast to all the 2D lamellar eutectic microstructures reported in the literature,[3–5,7,9,11,14,16–20] at a given location, while one side of the sample is covered by large γ(Sn) phase, the

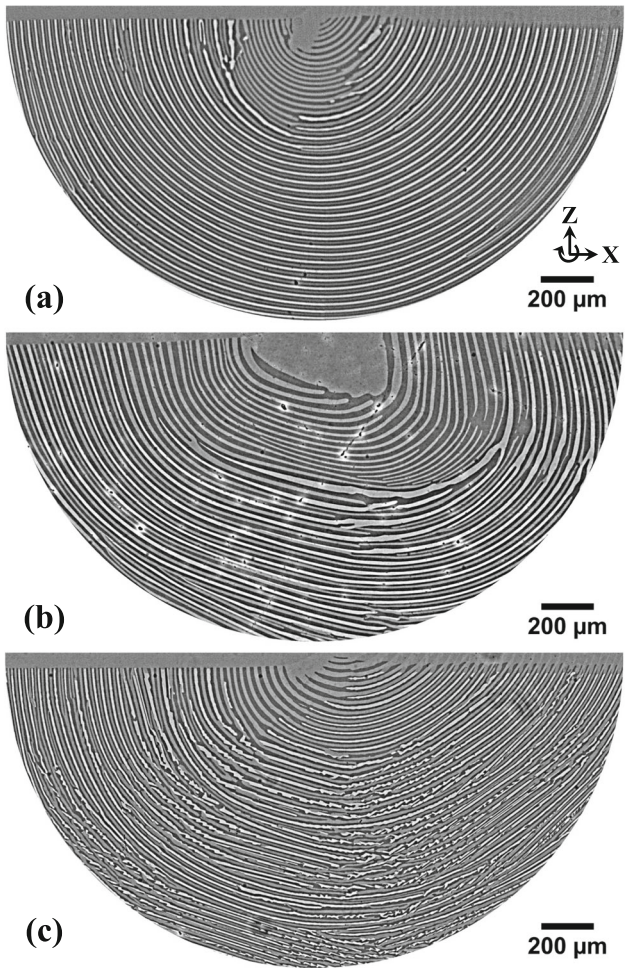


Fig. 3—Eutectic grain types observed in β(In)–In_2Bi–γ(Sn) system during RDS. δ = 13 μm. (*a*) Quasi-isotropic grain. ω = 0.019 deg/s. (*b*) Nearly-locked grain. ω = 0.006 deg/s. (*c*) Locked grain. ω = 0.015 deg/s. Microstructure evolves in CW direction.

alteration of the In_2Bi and β(In) phases exists on the other side, as shown in Figure 4. Thanks to the double-sided microscope, which is a unique equipment used to visualize the solidification front in real time from both sides of the sample, we could identify this difference indicating that the microstructure is completely 3D, despite the highly confined sample geometry. In this study, we name this new grain type as "Laminated Matrix with Rods" (LMR), where all three phases are growing at the same temperature, as in the case of the other eutectic grain types, meaning that the phases are growing in a coupled manner. The aspect ratio, *i.e.,* the ratio of the phase thickness in Y direction to its width in X direction, of the γ(Sn) phase in LMR is totally different from the ones observed in all other grain types reported in this system, namely quasi-isotropic, nearly-locked, and locked grains. Additionally, in the example shown in Figure 4, the characteristic inclination of the In_2Bi/β(In) interphase boundary and its straightness suggest a strong local minimum on the γ-plot, which gives rise to inclined two-phase AB pattern. The inclination angle was measured to be 21.8 ± 1.5 deg for microstructures grown at the velocity range of 0.08–0.18 μm/s. In other words, since the A/B interphase boundary is locked to a strong local minimum on the γ-plot, the inclination angle is not dependent on the growth velocity (within the employed range). More specifically, since the magnitude of A/B interphase energy is minimum at this orientation, experimental conditions such as growth velocity do not change the inclination angle. The tilt angle of the strongly anisotropic interphase boundary being constant with velocity change is an expected result.

To investigate the growth dynamics of LMR grains, interphase boundaries should be continuously rotated with respect to the temperature gradient direction. Therefore, we performed systematic RDS experiments to examine the evolution of LMR grains over the entire crystallographic orientation in 2D by changing the orientation of the sample continuously with respect to the direction of temperature gradient. In the upcoming sections, in order to characterize the LMR grains, onset of LMR state, microstructures evolution of the LMR grains, and phase morphologies in the LMR grains are presented.

A. *Onset of LMR State During RDS*

The onset of LMR state is investigated by rotating a directionally solidified microstructure obtained in another sample. In the example shown in Figure 5, the sample was directionally solidified until $\theta = 0$ deg and then, rotation was started with a constant angular speed. The image shown in Figure 5 was taken when rotation angle $\theta = 65$ deg. In this microstructure, two different grains, namely LMR (on left) and quasi-isotropic (on right), can be clearly identified. The microstructure at the growth front of the LMR grain (inset 1) is completely different from the quasi-isotropic grain with mostly ABAC arrangement (inset 3). Interestingly, both grains had the ABAC pattern with the same microstructural features including *(i)* having lamellar structure, *(ii)* all the interphase boundaries being parallel to the

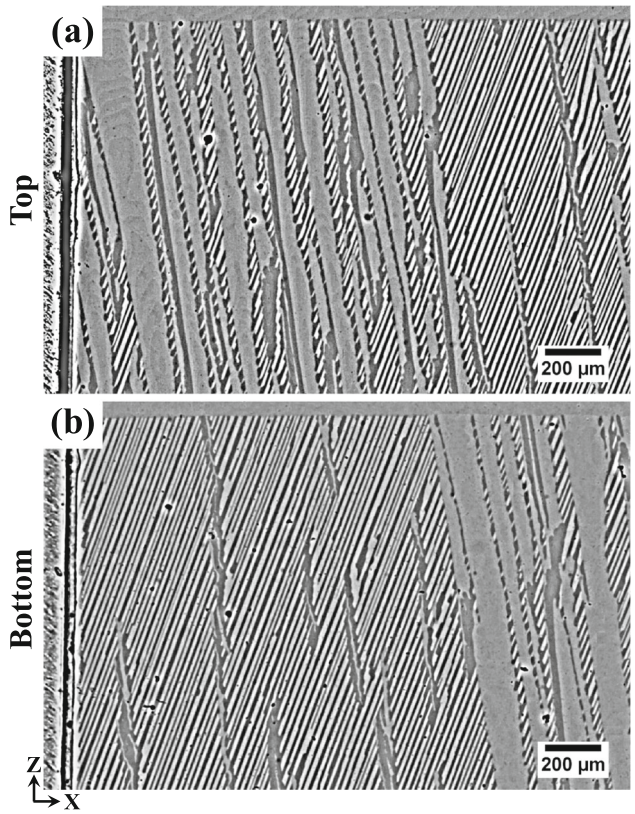


Fig. 4—The LMR eutectic grain microstructure with anisotropic In_2Bi/β(In) interphase boundary during a DS experiment. $V = 0.08$ μm/s, $\delta = 23$ μm. (*a*) Top view consists of mostly large γ(Sn) phases on the left side and alteration of In_2Bi and β(In) phases on right side of the image. (*b*) Bottom view showing alteration of In_2Bi and β(In) phases on the left side and large γ(Sn) phases on the right side of the image. On the left side of the images, the sample edge is visible.

imposed temperature gradient, *i.e.,* the triple-point junctions follow G, and hence present floating dynamics, *(iii)* eutectic spacing, defined as the width of ABAC pattern, and the width of each phase are comparable during DS (insets 2 and 4). Nonetheless, the disordered microstructure at the grain boundary (marked with the black dashed curve) gave a clue about the existence of different grains. During RDS, in the quasi-isotropic grain, the triple-point junctions follow the direction of the imposed temperature gradient and ABAC pattern continues to grow, while in the LMR grain, the onset of LMR state takes place by gradual enlarging of γ(Sn) regions through the elimination of many In_2Bi and β(In) phases, and triple-point junctions movement deviate from the G direction. Simultaneous growth of the LMR and the quasi-isotropic grains in a 2D sample growing at the same temperature, composition, temperature gradient, thickness, and similar growth velocities suggests that the differences in microstructures have crystallographic origins rather than being determined with the experimental conditions. Since in ABAC pattern, two kinds of interphase boundaries (A/B and A/C) exist, the crystallographic origin that results in the onset of LMR state can be related to In_2Bi/β(In) (A/B) and/or In_2Bi/γ(Sn) (A/C) boundaries.

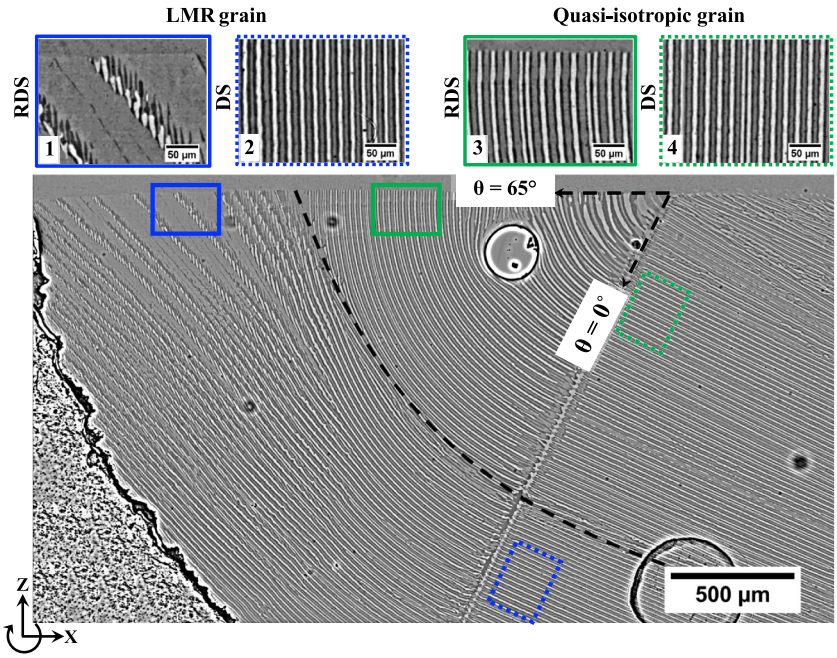


Fig. 5—Simultaneous growth of an LMR (on left) and a quasi-isotropic (on right) grains during DS and RDS (bottom view). The grain boundary is marked by a black dashed curve. Insets 1 and 2: LMR grain microstructures during RDS (after 65 deg rotation) and DS, respectively. Insets 3 and 4: Quasi-isotropic grain microstructures during RDS (after 65 deg rotation) and DS, respectively. $V = 0.6$ μm/s for DS, $\omega = 0.019$ deg/s for RDS, and $\delta = 13$ μm. A big bubble defect close to the center of rotation locally disturbed the ABAC pattern (Color figure online).

When LMR and quasi-isotropic grains shown in Figure 5 are further rotated 30 deg, the LMR grain evolved to AB pattern on the top microstructure and a large C (γ(Sn)) phase on the bottom microstructure, while the quasi-isotropic grain continued to have the ABAC pattern as shown in Figure 6 (a) and (b). Enlarged regions marked with blue rectangles from the top and bottom microstructures in the LMR grain are shown in inset images 1 and 3 along with the schematics of the LMR state (insets 2 and 4). The triple-point junctions in AB pattern (inset 1) follow the temperature gradient axis, indicating that In_2Bi/β(In) interphase boundary has floating dynamics, in contrast to the one observed in the LMR grain shown in Figure 4. Observation of LMR grain with A/B interphase boundaries having both floating and locked dynamics suggests that the responsible boundary for LMR is In_2Bi/γ(Sn) (A/C). In addition, this result shows that LMR grain can be obtained with different orientation relationships between In_2Bi and β(In) phases. Unfortunately, the interphase boundary energy anisotropy of the responsible boundary in LMR grains cannot be measured using the RDS pattern, due to the fact that the A/C boundaries disappear from both top and bottom views of the microstructure within the LMR state.

B. *Microstructure Evolution of the LMR Grain During RDS*

We now investigate the microstructure evolution of LMR grain by examining the top and bottom microstructures at different rotation angles. For the sake of simplicity, the LMR state microstructure with AB on the top and C phase on the bottom shown in Figure 7(a) is taken as the reference point, *i.e.,* the rotation angle is defined here as 0 deg. As sample rotates, while AB continues to present floating dynamics on top, anisotropic In_2Bi/γ(Sn) interphase boundaries formed on the bottom side (Figure 7(b)). Further rotation results in observation of all three phases on both sides of the sample (Figure 7(c)). With time, ABAC pattern forms on both sides and due to the anisotropic In_2Bi/γ(Sn) interphase boundaries, nearly-locked state is observed (Figure 7(d)). It should be highlighted here that in the nearly-locked state even though there are some 3D features during elimination and branching of phases, the growth morphology of all the phases is lamella. ABAC pattern rotates with sample in the nearly-locked state (Figure 7(e)) until it cannot grow any further. At this stage, the transient state takes place (Figure 7(f)) before reaching the second nearly-locked state. These nearly-locked states should correspond to two different non-singular minima in the interphase boundary γ-plot. By further rotation, γ(Sn) gets thicker on the top and narrower on the bottom (Figure 7 g)). Finally, γ(Sn) completely leaves the bottom side, the neighboring In_2Bi phases are merged, and many branching events occur (Figure 7(h)). Disappearance of the anisotropic In_2Bi/γ(Sn) interphase boundaries on the bottom side results in formation of AB pattern with floating dynamics. Hence, In_2Bi/β(In)/L triple-point junctions start to follow the imposed temperature gradient direction. On the top, β(In) disappeared, while traces of In_2Bi phase and hence the tilted and anisotropic In_2Bi/γ(Sn) interphase boundaries are still visible. After 180 deg rotation, LMR state formed again where

γ(Sn) is on the top and a relatively uniform AB pattern is on the bottom side of the sample. The formation of totally different microstructures with planar solid/liquid interfaces at the same temperature on top and bottom views in such a thin sample suggests that the morphology of all the phases changes with the formation of the LMR state. Frequent observation of different phases on one side of the thin sample in each 180 deg rotation is also remarkable. More specifically, while in the first LMR state, In_2Bi and β(In) phases grow on top, the γ(Sn) phase grows at the bottom. After 180 deg rotation of the sample, in the next LMR state, In_2Bi and β(In) phases grow at the bottom, while γ(Sn) phase grows on top. Such an observation demonstrates that the gravity does not have an effect on the evolution of the LMR grains.

To observe the microstructure of an LMR grain over the entire 2D crystallographic orientation, sample was rotated over 360 deg as shown in Figure 8 (top and bottom views). Real-time video showing microstructure evolution at the solidification front of the LMR grain during RDS from top and bottom (the same grain shown in Figures 7 and 8) is given in the Supplementary Material 2. The characteristic features of this LMR eutectic grain are summarized as follows: (*i*) It has two large axisymmetric LMR states within a well-defined angular range. Remarkably, while in the first LMR state, the bottom microstructure consists of the γ(Sn) phase, after 180 deg rotation, the AB pattern forms in the second LMR state. (*ii*) The full rotation contains two sets of axisymmetric nearly-locked states (NL_1 and NL_2) with mostly ABAC pattern. After each LMR state, a transition occurs to the nearly-locked state (NL_2), which is followed by another one (NL_1) through a smooth transient state. (*iii*) The transient from the nearly-locked to LMR state (or vice versa) occurs within an angular range where while the phases are rearranged, the phase morphologies change from 2D lamella in the nearly-locked state to a 3D configuration in LMR state.

C. *Phase Morphologies in LMR Grains*

In order to investigate the 3D configuration of all phases in the LMR state, a specific sample is prepared. For this sample, first an LMR state is reached during RDS, then the rotational movement is stopped and the sample is directionally melted until a seed of LMR grain is remained. At this moment, the sample is started to be directionally solidified. As a result, a quasi-isotropic grain (on left) and two different LMR grains (in the middle and on right) are obtained as shown in Figure 9. In LMR grains, γ(Sn) phase is observed on the bottom, while In_2Bi and β(In) phases are growing on top. In_2Bi/β(In) interphase boundaries in the middle grain are mostly parallel to the imposed temperature gradient axis, whereas they are highly inclined on the right grain. In other words, the In_2Bi/β(In) boundaries are quasi-isotropic and anisotropic in the middle and right LMR grains, respectively. Remarkably, each interphase boundary has its specific impact on the microstructure. While anisotropy in In_2Bi/γ(Sn) boundary results in LMR grain formation, depending on the interphase boundary energy function of the In_2Bi/β(In) interphase, floating or locked dynamics are observed at the In_2Bi/β(In) boundary within the LMR state. In the right grain, locked dynamical features including the formation of kinks on the interphase boundary and poor wetting properties between the β(In) phase and the sample wall at the solidification front[5] are observed. The existence of LMR grains with two different In_2Bi/β(In) boundaries proves once again that In_2Bi/γ(Sn) boundary is the responsible one for LMR grain formation. Additionally, observation of these two LMR grains within the same sample and the same experimental conditions is an extraordinary illustration indicating that depending on the interphase boundary energy function, two different anisotropic interphase boundaries, *i.e.,* In_2Bi/β(In) and In_2Bi/γ(Sn) can operate individually, affect the

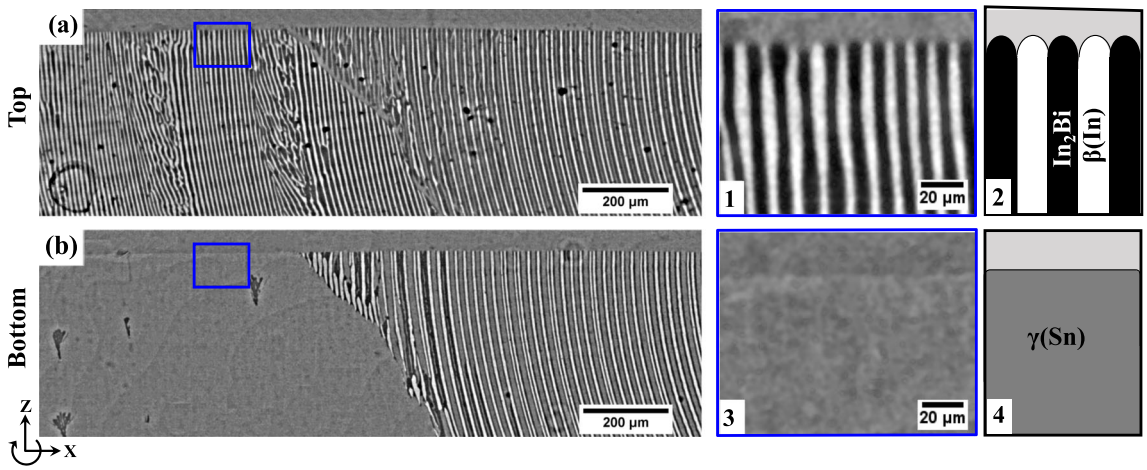


Fig. 6—Top and bottom microstructures obtained in LMR and quasi-isotropic grains after 95 deg rotation. (*a*) Top microstructure includes AB pattern in the LMR grain and ABAC pattern in the quasi-isotropic grain. (*b*) Bottom microstructure has a large C phase in the LMR grain and ABAC pattern in the quasi-isotropic grain. Small fractions of In_2Bi phases are observed within the γ(Sn) region in the LMR grain. Insets 1 & 3: Magnified images of AB pattern and C phase at the growth front of the LMR grain from the same XZ position. Insets 2 & 4: The schematic representations of top and bottom microstructures in an LMR state. $\omega = 0.019$ deg/s and $\delta = 13$ μm (Color figure online).

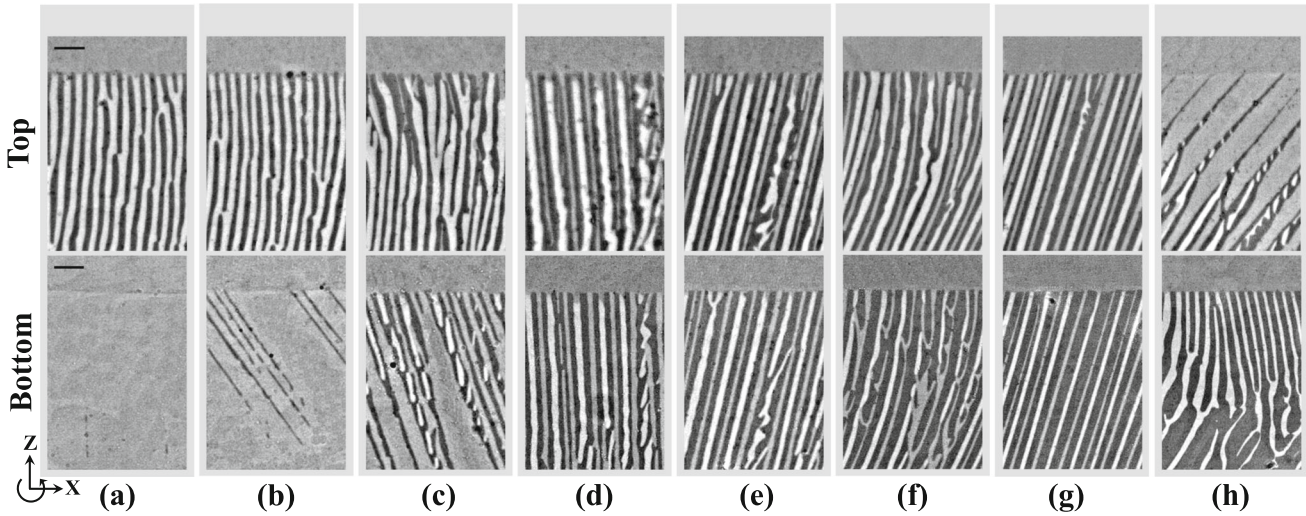


Fig. 7—Evolution of the LMR grain during RDS. (*a*) LMR state with fully 3D microstructure is observed with AB pattern on top and single γ(Sn) phase on the bottom microstructure, which is defined as the reference point, $\theta = 0$ deg. (*b*) After 12.0 deg rotation, the floating AB pattern continues to grow on top, while anisotropic In_2Bi/γ(Sn) interphase boundaries started to form on the bottom. (*c*) At $\theta = 27.0$ deg rotation, all three phases are present on both sides, (*d*) Nearly-locked ABAC pattern observed at $\theta = 40.6$ deg. (*e*) The inclined lamellar structure of the same nearly-locked state observed at $\theta = 55.6$ deg. (*f*) Transient microstructure between two nearly-locked states exists at $\theta = 79.1$ deg. (*g*) The inclined lamellar structure of the second nearly-locked state observed at $\theta = 109.1$ deg. (*h*) Onset of LMR state at $\theta = 134.1$ deg, where γ(Sn) phase is started to form on top and AB pattern on the bottom microstructure. $\omega = 0.010$ deg/s, $\delta = 13$ μm. Scale bar is 50 μm.

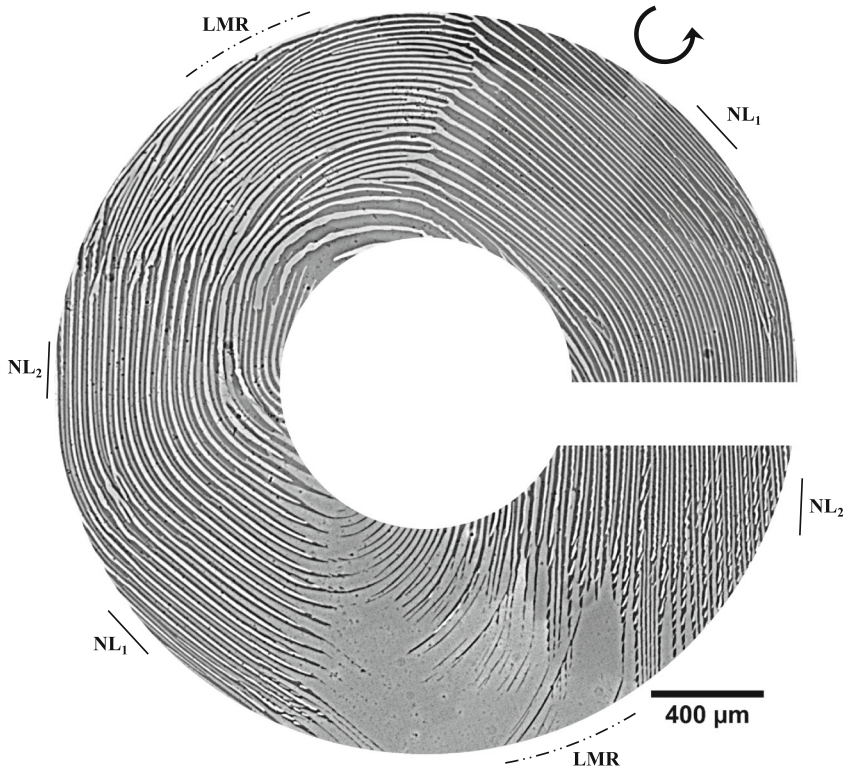
microstructure separately in their own way without interfering with each other.

In order to investigate the morphologies of each phase in these grains, a cross-section was metallographically prepared and images were taken under SEM (Figures 10 and 11). As explained in the *Experimental methods* section, in SEM-BSE images, the color of In_2Bi phase is light gray, while γ(Sn) and β(In) are both dark gray due to having similar densities. It should be mentioned here that when a cross-section is cut from the sample, the alloy exposed to air etches, and the interphase boundaries start corrugating.[33] In addition, Thermo-Calc simulations showed that the phase fractions significantly change going from eutectic to room temperature.[32] In the course of cooling, while In_2Bi mole fraction substantially increases, the ones for β(In) and γ(Sn) decrease. Due to these reasons, the microstructure and morphologies formed during solidification can only be captured to a certain extent by post-mortem analysis. Nevertheless, one can confirm the growth morphology of all the phases. In addition, Thermo-Calc simulations confirm that there is no solid-solid phase transformation after solidification.[32] Hence, crystallographic analysis can be performed at room temperature.

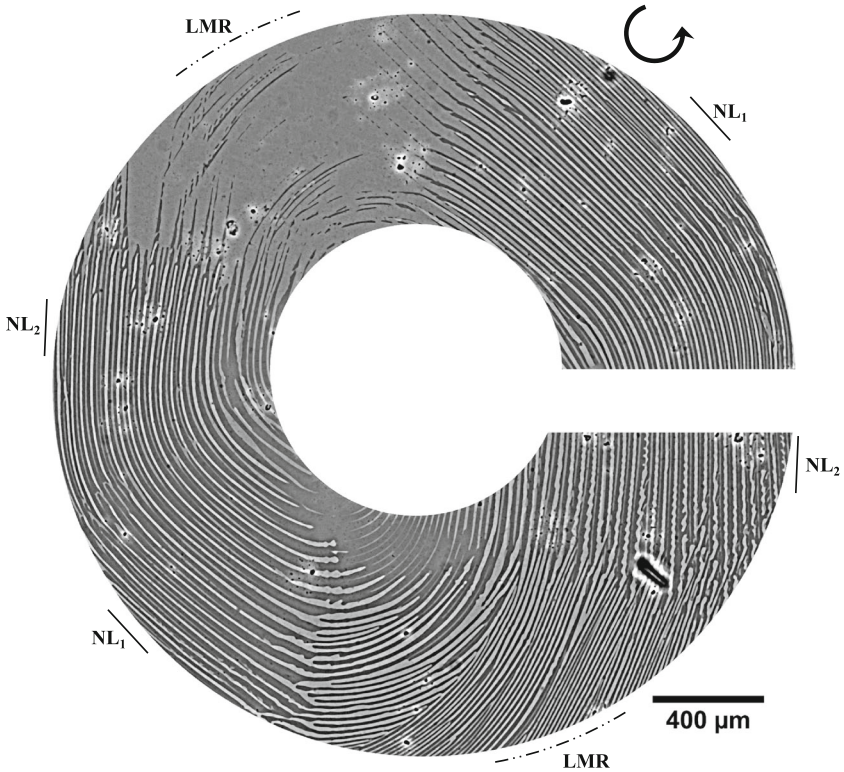
The cross-section microstructure of quasi-isotropic grain along with the schematic representation (including the identity of each phase and mirror symmetry planes (MP)) is shown in Figure 10. In this configuration, there are two mirror symmetry planes, named here as MP^1 and MP^2, which are at the center of β(In) and γ(Sn) phases, respectively. The interphase boundaries are nearly perpendicular to the sample walls, and they are extending from one sample wall to the other. Therefore, the microstructure is considered to be 2D lamellar structure.

In the LMR grains, the morphology of the phases and the direction of the interphase boundaries are totally different (Figure 11). The microstructure is completely 3D as the phases do not extend from one sample wall to the other, despite the strong confinement effect. In the microstructures shown in Figure 11, the In_2Bi phase forms the matrix, while γ(Sn) phase has lamellar morphology covering the bottom side of the sample and β(In) has contact only with top sample wall. In addition, in both of these grains, the In_2Bi/γ(Sn) boundary is perpendicular to the ones observed in the quasi-isotropic grain shown in Figure 10. Remarkably, since the γ(Sn) phase covers the sample wall, In_2Bi and β(In) phases lose their contact with one side of the sample wall, which in turn results in the In_2Bi/γ(Sn) boundary being parallel to the *X*-axis and the sample wall. This is in strong contrast with the eutectic microstructures observed in thin sample directional solidification experiments reported until now[3–5,9,11,14,16–20] wherein the interphase boundaries are always in contact with both sample walls and mostly parallel to the *Y* direction. In both of these LMR grains, the β(In)/γ(Sn) boundary does not exist as it was already reported for the other grain types observed in this system.[5,9,18,33,34]

The main difference in these LMR grains is the morphology of β(In) phase which is elongated rod when the In_2Bi/β(In) boundary is quasi-isotropic and trapezoid when In_2Bi/β(In) boundary is strongly anisotropic, as shown in Figures 11(a) and (b), respectively. In addition, the anisotropic In_2Bi/β(In) boundaries are tilted with respect to not only *Z* but also *Y*-axis as well. Furthermore, in the LMR grain with quasi-isotropic In_2Bi/β(In) boundary, there are two MPs. The *X* position of these planes is at the center of β(In) phase



(a)



(b)

Fig. 8—Full-turn rotation of an LMR grain viewed from (*a*) top and (*b*) bottom of the sample. The microstructure includes two LMR states and four nearly-locked (NL) states linked via transient states. The spots on the microstructure are dirt on the glass plate. $\omega = 0.010$ deg/s, $\delta = 13$ μm.

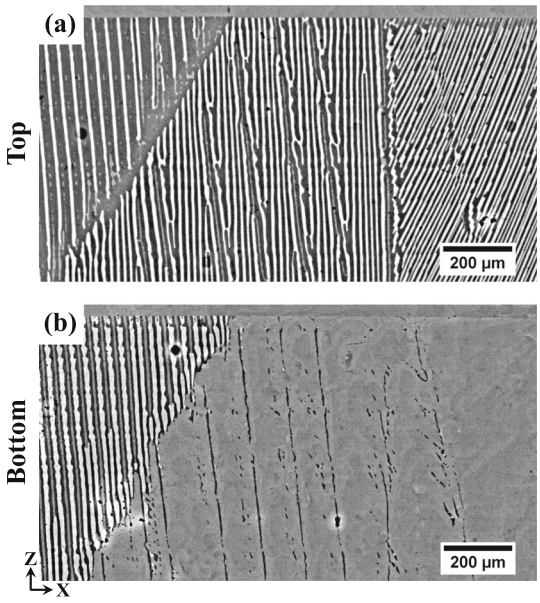


Fig. 9—A quasi-isotropic eutectic grain (on left) growing simultaneously with different types of LMR grains (in the middle and on right). (*a*) Top microstructure consists of a quasi-isotropic grain with ABAC-type growth pattern on the left side, LMR grain with In_2Bi/β(In) boundary mostly parallel to the temperature gradient direction in the middle, and another LMR grain with In_2Bi/β(In) boundary steeply inclined with respect to the temperature gradient direction on the right. (*b*) Bottom microstructure consists of a quasi-isotropic grain with ABAC-type growth pattern on the left side, and γ(Sn) phase region with some traces of In_2Bi phase in the middle and on right. On bottom microstructure, the grain boundary between the two LMR grains is not distinguishable. $\delta = 13$ μm and $V = 0.15$ μm/s.

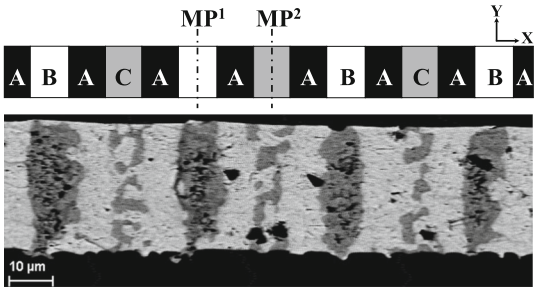


Fig. 10—The cross-sectional microstructure of the quasi-isotropic grain with ABAC-growth pattern obtained from the same sample as the one shown in Fig. 9 along with the schematic representation. All phases have lamellar growth morphology. $V = 0.15$ μm/s.

and at the middle of the two nearest neighboring β(In) phases. The symmetry in the LMR grain with anisotropic In_2Bi/β(In) boundary is entirely broken due to the tilt of the In_2Bi/β(In) boundary with respect to *Y*-axis. Despite the considerable differences in the mirror symmetry conditions and morphology of the phases, observation of the solidification fronts of all three grains growing at the same temperature suggests that LMR grains also provide efficient solute exchange during growth.

Determination of the morphologies in the LMR state and knowing that all the phases in LMR grains have lamellar morphology at the nearly-locked states suggest that morphological transitions occur during RDS of LMR grains. These morphological transitions, which are dictated by the interphase boundary anisotropy, are reproducible and occur at each and every 180 deg rotation of the sample. Going from nearly-locked to LMR state, while the morphological transition of the β(In) phase from lamellae to elongated/trapezoidal rod structure occurs, the In_2Bi/γ(Sn) boundary rotates 90 deg, *i.e.,* it becomes parallel to *X*-axis. The morphological changes of β(In) phases from lamellae to elongated/trapezoidal rod can be recognized as a lamella to rod transition originated from the interphase boundary energy anisotropy. In other words, these morphological transitions, which are the unique features of LMR grains, are not due to a change in experimental condition, as typically reported in the literature, but it is only due to the special crystal/crystal orientation relationships. From all of these observations, it is concluded that the anisotropy in In_2Bi/γ(Sn) interphase boundary energy alters the morphologies of phases and leads to the formation of this new and particular three-phase eutectic grain type.

Since In_2Bi/γ(Sn) interphase boundary is parallel to the *XZ* plane (*i.e.,* normal to *XY* plane), during the LMR state, the interphase boundary trace, *i.e.,* equilibrium shape, of the A/C interphase boundary could not be obtained for LMR grains, as it was done, for example, for nearly-locked grains in Reference 9. Nevertheless, the observation of reproducible and symmetric LMR states within the RDS pattern proves that the anisotropy of the In_2Bi/γ(Sn) interphase boundary energy results in LMR grain formation.

IV. DISCUSSION

To examine the microstructure of LMR grain with the quasi-isotropic In_2Bi/β(In) boundaries in an extended geometry, we introduced reflective boundary conditions at the sample walls as shown in Figure 12. In this representation, two additional mirror planes, $MP^1{}_x$ and $MP^2{}_x$, exist due to the reflective boundary conditions along the *X* direction. Hence, this pattern is suggested to be one of the 3D steady-state microstructures of three-phase eutectic systems. The morphology and the arrangement of the phases in this system are different from the three-phase solidification microstructures observed in numerical and experimental studies[35–40] and other self-organized systems such as triblock copolymers.[41] The difference arises from the fact that in the studied system, two of the phases, namely γ(Sn) and β(In), never come in contact, which results in having only two interphase boundaries instead of three. Similar structures, however, are formed in composite materials. Inspired from composite structures, we name this specific microstructure as "Laminated Matrix with Rods" (LMR), where In_2Bi is the matrix, rods are β(In), and "laminate" is γ(Sn).

As the interphase energy anisotropy of the In_2Bi/γ(Sn) boundary is shown to be responsible for the morphological transitions, the crystal orientations of In_2Bi and γ(Sn) phases and hence the orientation relationships

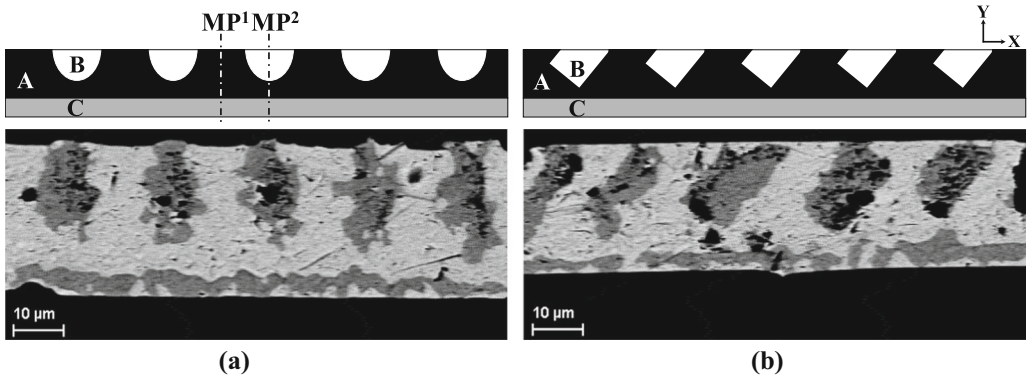


Fig. 11—The cross-sectional microstructure of two types of LMR grains obtained from the same sample as the one shown in Fig. 9 along with their schematic representations. (*a*) LMR grain with the quasi-isotropic $In_2Bi/\beta(In)$ boundaries. (*b*) LMR grain with anisotropic $In_2Bi/\beta(In)$ boundaries. $V = 0.15$ μm/s.

should be different from the ones obtained in quasi-isotropic and locked grains. In a previous study, the special ORs in the quasi-isotropic and locked eutectic grains in the $\beta(In)$–In_2Bi–$\gamma(Sn)$ system were determined using EBSD technique.[20] Remarkably, it was found that the (0001) plane, *i.e.,* the basal plane, of both $\gamma(Sn)$ and In_2Bi phases is completely parallel to the sample wall (*XZ* plane) in the locked grain, while the same plane in $\gamma(Sn)$ and In_2Bi phases is parallel and nearly parallel to the *XZ* plane, respectively, in the quasi-isotropic grain. Since one side of the sample is totally covered by $\gamma(Sn)$ phase within LMR state, there should be a specific orientation of $\gamma(Sn)$ phase with respect to the sample wall. A preliminary study on the orientation of the phases within an LMR grain revealed that in a strong contrast to the quasi-isotropic and locked eutectic grains, the basal plane of $\gamma(Sn)$ phase is perpendicular to the sample plane. In other words, $\gamma(Sn)$ phase oriented in a way that $(11\ \bar{2}\ 0)$ plane of the hexagonal lattice lies parallel to the sample plane. It is suggested here that the formation of LMR grains may originate from the specific orientation of this phase with respect to the sample wall and therefore leads to a particular type of anisotropy of $In_2Bi/\gamma(Sn)$ interphase boundary. On the other hand, the basal plane of In_2Bi phase in LMR grain is nearly parallel to the sample plane, as in the case of quasi-isotropic grain. Due to the orientation difference of the phases, there should be different ORs in LMR grains compared to quasi-isotropic and locked eutectic grains. Complementary studies to establish the overall ORs in all types of grains observed in this system are under investigation.

Since both $\gamma(Sn)$ and In_2Bi phases were grown from the as-cast microstructure and no nucleation was observed during DS and RDS experiments for these two phases, the orientations of these crystals and the ORs in eutectic grains must originate from the sample filling process, where heterogeneous nucleation on the glass sample wall may create a specific relation between the basal plane of hexagonal phases and *XZ* plane. Subsequently, one phase nucleating onto the other one and competitive growth after the sample filling process result in various crystal orientations and grains in the sample.

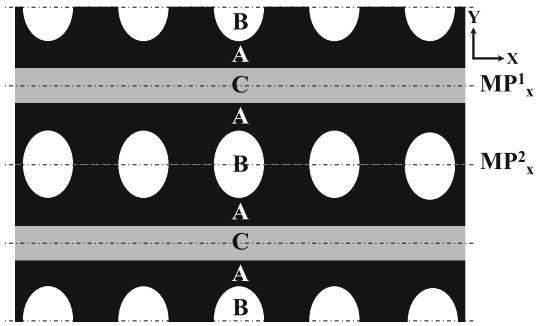


Fig. 12—Extended geometry of the LMR state with quasi-isotropic $In_2Bi/\beta(In)$ interphase boundaries. $MP^1{}_x$ and $MP^2{}_x$ are the mirror planes.

V. CONCLUSION

In this study, we introduce a new class of three-phase eutectic grain entitled as "Laminated Matrix with Rods" (LMR), thanks to the RDS experiments along with the unique double-sided microscope setup designed in-house specifically to investigate the real-time solidification dynamics in metals. In LMR grains, within a well-defined angular range, while $\gamma(Sn)$ phase completely covers one side of the sample, In_2Bi and $\beta(In)$ phases grow on the other side, despite the thin sample geometry. We show for the first time in the literature that systematic and periodic morphological transitions occur when the orientation of the interphase boundaries is changed with respect to G direction. More specifically, In_2Bi, $\beta(In)$, and $\gamma(Sn)$ phases exhibit lamella to matrix, lamella to elongated/trapezoid rod, and lamella perpendicular to *X*-axis to lamella parallel to *X*-axis transitions (and vice versa) periodically during RDS experiments. In LMR grains, observation of anisotropic $In_2Bi/\gamma(Sn)$ interphases (Figure 7(b)), obtaining floating dynamics

on In_2Bi/β(In) boundaries when In_2Bi/γ(Sn) interphase disappears on one side of the sample (Figure 7(h)), and observation of both floating and locked dynamics on In_2Bi/β(In) boundaries in LMR grains lead to the conclusion that the In_2Bi/γ(Sn) is the responsible boundary for LMR grain formation. Growth of the LMR grain at the same temperature next to a quasi-isotropic grain confirms that the growth is coupled and the microstructure selection is not due to experimental parameters such as composition, growth velocity, temperature gradient, sample thickness, but originates from interphase boundary anisotropy. Another interesting feature of LMR grains is that within two axisymmetric LMR states that are following each other, two different phase arrangements are observed on one side of the sample in all of our experiments with LMR grains. More specifically, in an LMR state, when only γ(Sn) is observed on top, for example, the upcoming LMR state has In_2Bi and β(Sn) phases on the same side of the sample. Such an observation demonstrates that segregation due to gravity is negligible and it does not affect LMR grain growth dynamics. In addition, it is illustrated that two different anisotropic interphase boundaries, *i.e.,* In_2Bi/β(In) and In_2Bi/γ(Sn), can have their own effect on the microstructure and operate individually without interfering with each other.

Last, but not the least, observation of a regular microstructure, such as the ABAC pattern, does not guarantee the absence of interphase boundary anisotropy. The current study demonstrates that a regular pattern might evolve to an extraordinary microstructure if the orientation of the interphase boundary is changed with respect to G. Thus, the importance of the RDS technique and real-time investigation in understanding the fundamentals of solidification and the microstructure evolution is proven once again.

ACKNOWLEDGMENTS

We thank S. Bottin-Rousseau, U. Hecht, S. Akamatsu, G. Faivre, and V. Witusiewicz for many fruitful discussions. We are greatly indebted to U. Hecht for her help in EBSD measurements and the determination of the orientation relationships. We acknowledge the assistance of V. Witusiewicz for Thermo-Calc calculations of the In-Bi-Sn system. This work was supported by European Commission Marie Curie Career Integration Grant No. FP7-PEOPLE-2012-CIG (NEUSOL 334216) and TÜBİTAK 3501 (Grant No. 212M013).

CONFLICT OF INTEREST

On behalf of all authors, the corresponding author states that there is no conflict of interest.

FUNDING

Open access funding provided by the Scientific and Technological Research Council of Türkiye (TÜBİTAK).

OPEN ACCESS

This article is licensed under a Creative Commons Attribution 4.0 International License, which permits use, sharing, adaptation, distribution and reproduction in any medium or format, as long as you give appropriate credit to the original author(s) and the source, provide a link to the Creative Commons licence, and indicate if changes were made. The images or other third party material in this article are included in the article's Creative Commons licence, unless indicated otherwise in a credit line to the material. If material is not included in the article's Creative Commons licence and your intended use is not permitted by statutory regulation or exceeds the permitted use, you will need to obtain permission directly from the copyright holder. To view a copy of this licence, visit http://creativecommons.org/licenses/by/4.0/.

SUPPLEMENTARY INFORMATION

The online version contains supplementary material available at https://doi.org/10.1007/s11661-024-07389-6.

REFERENCES

1. J. Hunt and D. Hurle: *Trans. Metall. Soc. AIME*, 1968, vol. 242, pp. 1043–47.
2. B. Caroli, C. Caroli, G. Faivre, and J. Mergy: *J. Cryst. Growth*, 1992, vol. 118, pp. 135–50.
3. S. Akamatsu, S. Bottin-Rousseau, M. Şerefoğlu, and G. Faivre: *Acta Mater.*, 2012, vol. 60, pp. 3206–14.
4. S. Akamatsu, S. Bottin-Rousseau, M. Serefoglu, and G. Faivre: *Acta Mater.*, 2012, vol. 60, pp. 3199–3205.
5. S. Mohagheghi and M. Şerefoğlu: *Acta Mater.*, 2018, vol. 151, pp. 432–42.
6. P. Steinmetz, A. Dennstedt, M. Şerefoğlu, I. Sargin, A. Genau, and U. Hecht: *Acta Mater.*, 2018, vol. 157, pp. 96–105.
7. S. Bottin-Rousseau, O. Senninger, G. Faivre, and S. Akamatsu: *Acta Mater.*, 2018, vol. 150, pp. 16–24.
8. U. Hecht, J. Eiken, S. Akamatsu, and S. Bottin-Rousseau: *Acta Mater.*, 2019, vol. 170, pp. 268–77.
9. S. Mohagheghi and M. Şerefoğlu: *Metall. Mater. Trans. A*, 2019, vol. 50, pp. 5221–33.
10. S.K. Aramanda, S. Khanna, S.K. Salapaka, K. Chattopadhyay, and A. Choudhury: *Metall. Mater. Trans. A*, 2020, vol. 51, pp. 6387–6405.
11. S. Bottin-Rousseau, M. Medjkoune, O. Senninger, L. Carroz, R. Soucek, U. Hecht, and S. Akamatsu: *J. Cryst. Growth*, 2021, vol. 570, 126203.
12. J. Friess, P. Rayling, U. Hecht, and A. Genau: *J. Cryst. Growth*, 2022, vol. 595, art. no. 126799.

13. R.E. Napolitano and S. Liu: *Phys. Rev. B*, 2004, vol. 70, art. no. 214103.
14. S. Ghosh, A. Choudhury, M. Plapp, S. Bottin-Rousseau, G. Faivre, and S. Akamatsu: *Phys. Rev. E*, 2015, vol. 91, art. no. 022407.
15. K.D. Noubary, M. Kellner, and B. Nestler: *Materials*, 2022, vol. 15, art. no. 1160.
16. S. Bottin-Rousseau, M. Serefoglu, S. Akamatsu, and G. Faivre: *IOP Conf. Ser. Mater. Sci. Eng*, 2012, vol. 27, art. no. 012088.
17. M. Medjkoune, S. Bottin-Rousseau, L. Carroz, G. Prévot, B. Croset, J.S. Micha, and S. Akamatsu: *IOP Conf. Ser. Mater. Sci. Eng*., 2023, vol. 1274, art. no. 012037.
18. S. Bottin-Rousseau, M. Şerefoğlu, S. Yücetürk, G. Faivre, and S. Akamatsu: *Acta Mater*., 2016, vol. 109, pp. 259–66.
19. S. Mohagheghi and M. Şerefoğlu: *J. Cryst. Growth*, 2017, vol. 470, pp. 66–74.
20. S. Mohagheghi, U. Hecht, S. Bottin-Rousseau, S. Akamatsu, G. Faivre, and M. Şerefoğlu: *IOP Conf. Ser. Mater. Sci. Eng*., 2019, vol. 529, art. no. 012010.
21. L. Rátkai, G.I. Tóth, L. Környei, T. Pusztai, and L. Gránásy: *J. Mater. Sci*., 2017, vol. 52, pp. 5544–58.
22. A. Choudhury, M. Plapp, and B. Nestler: *Phys. Rev. E*, 2011, vol. 83, art. no. 051608.
23. W. Kurz and D.J. Fisher: *Fundamentals of Solidification*, Trans Tech Publications, Uetikon-Zuerich, 1998.
24. M. Serefoglu and R.E. Napolitano: *Acta Mater*., 2008, vol. 56, pp. 3862–73.
25. M. Şerefoğlu and R.E. Napolitano: *Acta Mater*., 2011, vol. 59, pp. 1048–57.
26. M. Serefoglu, S. Bottin-Rousseau, S. Akamatsu, and G. Faivre: *IOP Conf. Ser. Mater. Sci. Eng*., 2012, vol. 27, art. no. 012030.
27. M. Şerefoğlu, S. Bottin-Rousseau, and S. Akamatsu: *Acta Mater*., 2023, vol. 242, art. no. 118425.
28. S. Akamatsu, S. Bottin-Rousseau, M. Şerefoğlu, V.T. Witusiewicz, U. Hecht, and M. Plapp: *C. R. Acad. Sci*., 2023, vol. 2, pp. 219–31.
29. A. Parisi and M. Plapp: *EPL*, 2010, vol. 90, art. no. 26010.
30. S. Khanna, S.K. Aramanda, and A. Choudhury: *Metall. Mater. Trans. A*, 2020, vol. 51, pp. 6327–45.
31. V.T. Witusiewicz, U. Hecht, B. Bottger, and S. Rex: *J. Alloys Compd*., 2007, vol. 428, pp. 115–24.
32. *Private communication with Dr. Witusiewicz*.
33. V.T. Witusiewicz, U. Hecht, S. Rex, and M. Apel: *Acta Mater*., 2005, vol. 53, pp. 3663–69.
34. S. Rex, B. Bottger, V. Witusiewicz, and U. Hecht: *Mater. Sci. Eng. A*, 2005, vol. 413, pp. 249–54.
35. R.J. Contieri, C.T. Rios, M. Zanotello, and R. Caram: *Mater Charact*, 2008, vol. 59, pp. 693–99.
36. A. Dennstedt and L. Ratke: *Trans. Indian Inst. Met*., 2012, vol. 65, pp. 777–82.
37. A. Choudhury: *Trans. Indian Inst. Met*., 2015, vol. 68, pp. 1137–43.
38. A. Choudhury, Y.C. Yabansu, S.R. Kalidindi, and A. Dennstedt: *Acta Mater*., 2016, vol. 110, pp. 131–41.
39. J. Hötzer, P. Steinmetz, A. Dennstedt, A. Genau, M. Kellner, I. Sargin, and B. Nestler: *Acta Mater*., 2017, vol. 136, pp. 335–46.
40. S. Khanna and A. Choudhury: *Metall. Mater. Trans. A*, 2021, vol. 52, pp. 4246–63.
41. R. Stadler, C. Auschra, J. Beckmann, U. Krappe, I. Voight-Martin, and L. Leibler: *Macromolecules*, 1995, vol. 28, pp. 3080–97.

Publisher's Note Springer Nature remains neutral with regard to jurisdictional claims in published maps and institutional affiliations.